Astrophysical Bulletin, 2009, 64, 272–279

Tessellated Mapping of Cosmic Background Radiation Correlations and Source Distributions

O.V. Verkhodanov[a], M.L. Khabibullina[a], E.K. Majorova[a]

Special Astrophysical Observatory of the Russian AS, Nizhnij Arkhyz 369167, Russia

Received 13 October, 2008; accepted 1 December, 2008.

We offer a method of correlations mapping on the full celestial sphere that allows to check the quality of reconstructed maps, their non-Gaussianity and conduct experiments in various frequency ranges. The method was evaluated on the WMAP data, both on the reconstructed maps and foreground components, and on the NRAO VLA Sky Survey (NVSS) data. We detected a significant shift in the correlation data of the dust component, which can be preconditioned by a more complex dust model than the one currently in use for component separation. While studying the NVSS correlation data, we demonstrated that the statistics of the coinciding spots in the microwave background and in the NVSS survey corresponds to the one expected in the ΛCDM model. This can testify for a chance coincidence of the spots in the NVSS and WMAP data in the CMB Cold Spot region. Our method is software-implemented in the GLESP package.
PACS: 95.75.-z, 98.62.Ve, 98.70.Dk, 98.70.Vc, 98.80.-k

1. INTRODUCTION

Full celestial sphere surveys in different frequency ranges have led to a major advance in the research of global properties of the world around us. Such important matters as determining the cosmological parameters of the Universe in its early stages, the formation of the large-scale structure of the Universe and the phenomenon of dark energy are among them. The observations of the cosmic microwave background radiation (CMB) by the Wilkinson Microwave Anisotropy Probe[1] (WMAP) [1, 2, 3], were revolutionary in modern cosmology. The data were recorded in five bands: 23 GHz (the K-band), 33 GHz (the Ka-band), 41 GHz (the Q-band), 61 GHz (the V-band) and 94 GHz (the-W band) with the measurements of intensity and polarization. The result of the analysis of these data were the CMB maps of anisotropy and polarization, the maps of foreground components (synchrotron and free-free emission, dust radiation), their power spectrum were as well deduced. For the harmonics of not very high order ($\ell < 100$), a map of CMB anisotropy distribution is listed, reconstructed from the multifrequency observations of foreground components implementing the Internal Linear Combination (ILC) method [1].

In present-day full sphere observations, the infrared [4], radio [5] and optical [6] wavelength ranges survey maps are actively used along with the microwave background data. With the aid of correlation between the CMB and radio emission, one can study both the contribution of radio sources into the common background [7, 8], and the correlation properties of the radio source and CMB distribution occurring both on the large scale ($\theta > 2^\circ$), like the Sachs-Wolfe effect [9], and on the small scale (mainly $\theta < 4'$) [10], like the Sunyaev-Zel'dovich effect. Correlations of infrared and optical surveys (specifically with known red shifts) with CMB data allow us to study the formation of a large-scale structure.

Another important application of correlation methods are studies of CMB maps quality and their cleaning level from other kinds of radiation. For example, the presence of correlation between the CMB and foreground components [11, 12] carried in by the Galaxy, points to a residual contribution of the interfering emission in the procedure of components separation. Therewith, the presence of correlated components in a number of multipole frequency ranges leads to a change in the CMB signal statistics, that manifests itself through non-Gaussianity [13]. That, in its turn, makes the analysis of the maps of the studied signal and their power spectrum more complex. Quite a significant number of papers has been dedicated to the studies of statistic properties of the signal on the ILC map and to the discussion of its non-Gaussianity. These works were conducted using different methods,

[1] `http://lambda.gsfc.nasa.gov`

like the phase analysis method [12, 13, 14], Maxwell's multipole vectors method [15], wavelet analysis [16, 17, 18] and Minkowski functionals [19, 20]. In the non-Gaussianity studies, the correlation method allows separating a non-Gaussianity of a certain type, e.g. the one preconditioned by systematization during data processing.

In this paper we generalize the approach of map correlation in various angular scales, earlier described in [21, 22]. We offer a method of tessellated mapping and maps correlation visualisation on the full sphere for different angular scales of correlation search. We use this approach for the construction and study of the ILC and WMAP5 foreground components correlation maps, where the WMAP data are from the fifth year of observations [2]; as well as for the correlation maps of ILC and NRAO VLA Sky Survey (NVSS) radio sources [5].

2. THE METHOD OF CORRELATIONS MAPPING

The correlation of two maps on the sphere is described by a correlation coefficient for a multipole ℓ as follows

$$K(\ell) = \frac{1}{2}\frac{\sum\limits_{m=-\ell}^{l} t_{\ell m}s^*_{\ell m} + t^*_{\ell m}s_{\ell m}}{(\sum\limits_{m=-\ell}^{l}|t_{\ell m}|^2 \sum\limits_{m=-\ell}^{\ell}|s_{\ell m}|^2)^{1/2}}\,, \qquad (1)$$

where $t_{\ell m}$ and $s_{\ell m}$ are the variations of CMB temperature and some other signal in a harmonic representation, * is a symbol of conjugation, ℓ and m are the numbers of spherical harmonics (of the multipole) and its modes in a harmonic decomposition of the signal on the sphere:

$$S(\theta,\phi) = \sum_{\ell}^{\ell_{max}}\sum_{m=1}^{\ell}\left(a_{\ell,m}Y_{\ell,m}(\theta,\phi) + a_{\ell,-m}Y_{\ell,-m}(\theta,\phi)\right)\,, \qquad (2)$$

where $Y_{\ell,m}$ are the spherical functions, (θ,ϕ) are the spherical coordinates, $a_{\ell,m}$ are the coefficients of spherical harmonics satisfying the following condition

$$Y_{\ell,-m}(\theta,\phi) = (-1)^m Y^*_{\ell,m}(\theta,\phi),$$
$$a_{\ell,m} = (-1)^m a^*_{\ell,-m}\,. \qquad (3)$$

The value of the $K(\ell)$ coefficient allows to check the harmonics correlation on the sphere, i.e. to compare the properties of maps in a given angular scale. However, while looking for the correlated regions which do not recur in other regions of the sphere, this approach brushes out such single areas while common averaging over the sphere within one harmonic. In this case it is practically impossible to separate the correlated regions.

We offer an approach realized within the framework of the GLESP package [23, 24], which allows detecting the correlations in the studied areas of a given angular scale for the maps, pixelized with higher resolution. The method is implemented in the pixel parametric space. The correlation mapping consists of assigning the pixel number p with a correlation result inside the solid angle Ξ_p, calculated for two maps having higher resolution. As a result, we obtain a new map, in which the value assigned to each pixel reflects the correlation level of the studied maps in a given area.

The correlation coefficient of anisotropy of the CMB temperature and a given signal for every pixel p ($p = 1, 2, ..., N_0$, where N_0 is the total number of pixels on the sphere), corresponding to the solid angle Ξ_p and deduced for the maps on the sphere with an initial resolution, determined ℓ_{max} (hereafter the value of $\ell_{max} = 150$ is taken for the original maps), there are

$$K(\Xi_p|\ell_{max}) = \frac{\sum\limits_{p_{ij}\in\Xi_p}\sum (\Delta T(\theta_i,\phi_j) - \overline{\Delta T(\Xi_p)})(S(\theta_i,\phi_j) - \overline{S(\Xi_p)})}{\sigma_{\Delta T_p}\sigma_{S_p}}\,, \qquad (4)$$

where $\Delta T(\theta_i,\phi_j)$ is the anisotropy value of the CMB temperature in a pixel with the coordinates (θ_i,ϕ_j) for the given pixelization resolution of the sphere, $S(\theta_i,\phi_j)$ is the value of another signal in the same area, $\overline{\Delta T(\Xi_p)}$ and $\overline{S(\Xi_p)}$ are common values in the area Ξ_p, deduced on the data from the maps with a higher resolution, plotted by ℓ_{max}, $\sigma_{\Delta T_p}$ and σ_{S_p} are the corresponding standards for this area.

3. CORRELATION MAPS OF ILC WMAP5 AND FOREGROUND COMPONENTS

One of the applications of the given approach is checking the cleaning quality of the CMB signal isolated from multifrequency observations. The presence of a residual (correlated) signal in the CMB data may lead to a bias in power estimation in a number of multipole ranges [25], which in its turn leads to a decrease in accuracy while determining the cosmological parameters.

Using the WMAP data—a map of synchrotron radiation in the K-band, a map of free-free emission in the V-band, dust radiation in the W-band and, finally, the ILC map—we have built correlation maps of foreground radiations and ILC at different angular scales.

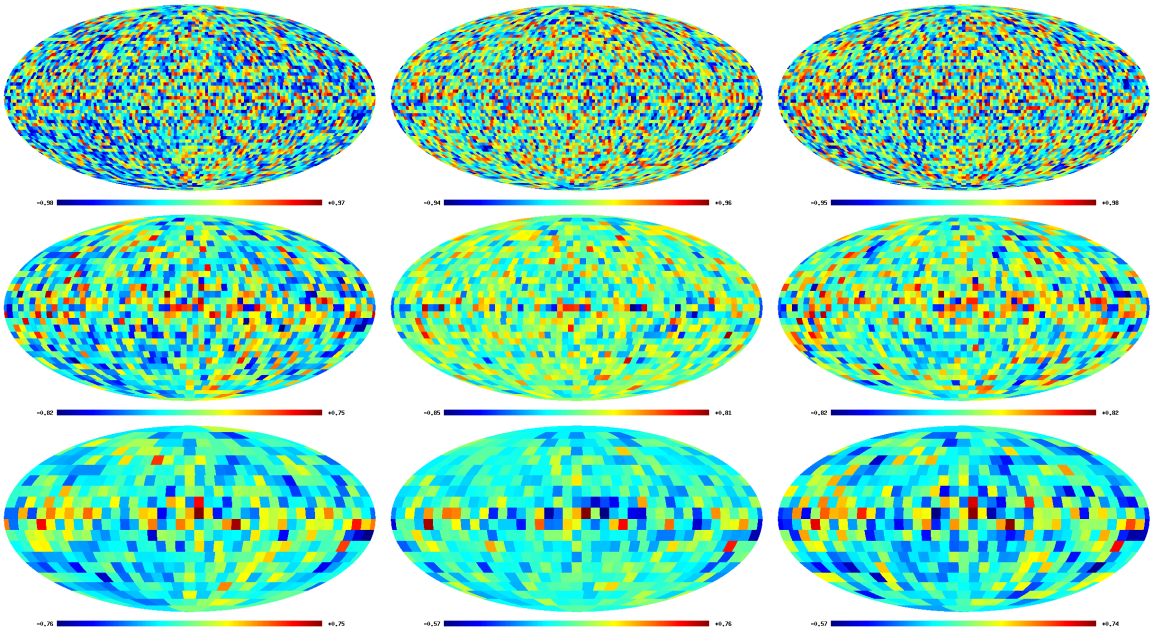

Figure 1: *Correlation maps of ILC and galactic foregrounds: dust, free-free and synchrotron radiation (from left to right), for different correlation windows: 162′, 324′ and 540′ (from top to bottom). The tone of the pixels reflects the value of the correlation coefficients from –1.0 to 1.0. The brighter the tone the smaller the absolute value of the correlation coefficient.*

As it was demonstrated earlier in the literature dedicated to the analysis of the ILC map and its signal statistics [11, 12, 13], there are some serious arguments for the fact that in this map at different angular scales there exists some residual contribution of foreground components, which, among other factors, gives the found non-Gaussianity. This contribution may as well manifest itself in the earlier discovered connection in the quadrupole between a cleaned map of the microwave background and galactic radiation components [25, 26, 27]. According to the papers of the WMAP team [1, 2], the ILC map is not intended for the CMB study on high multipoles, but it could be used for a foreground components analysis. This is the map we use for the foreground properties analysis.

In our previous work [21], using one-dimensional sections, we employed a WMAP mission foreground maps correlation search approach, and discovered in particular, that in the WMAP maps sections on declination $\delta = 41^\circ$ there is a signal, correlated and anti-correlated with the data of the components being separated. Among other things, on the angular scales indicative for the Galactic plane (multipole range ℓ=10–20) some notable, compared to the simulated maps, correlations with the galactic foreground components were discovered. These correlations may be the consequence of the residual errors at the signal separation phase.

In the present work we constructed the ILC and WMAP5 foreground components correlation maps on the full sphere. We as well estimated here the statistical value of the isolated correlated areas using the Monte-Carlo method, comparing them with the Gaussian random fields maps, generated on full celestial sphere for the ΛCDM cosmological model [3]. The results of correlation mapping of the ILC and galactic foreground maps are demonstrated in Fig. 1 for the correlation windows with the sides of 162′, 324′, 540′ (consequently, ℓ_{max_1} = 33, 16, and 10) for the three phase components. The window dimensions were chosen in such a manner that they fit into the range of angular scales of the Galaxy's influence (ℓ=10–20), and the possible Sachs-Wolfe effect ($\ell \leq 45$).

The Galactic plane can clearly be seen on the maps presented in Fig.1. An important marker here is the correlation value statistics for every pixel. We constructed the histograms for all the given maps and compared them with analogous results for the simulated maps. The simulated maps were generated with an assumption that the CMB data are the result of a Gaussian random process with an angular power spectrum, corresponding to the cosmological ΛCDM model. In total, there were constructed 50 random simulated maps using the *cl2map* procedure of the GLESP package [23, 24], and with their aid we were able to evaluate the admissible interval, de-

termined by the correlation values spread dispersion. The pixel value distribution is presented in Fig. 2. The admissible limits of the correlation level constructed on the modelling data, are shown with dashed lines.

Two foreground components correlations, dust and synchrotron, exhibit a shift in the range of anti-correlations. While in case of the dust component this shift is observed in all the studied scales, in case of synchrotron radiation it is presented on the histograms for $324'$ and $540'$. The free-free emission histogram shows the distribution within the normal range, corresponding to CMB as a Gaussian random process. We have to note, that an analogous shift in the distribution was detected for low multipoles at the analysis of the ILC signal reconstruction method [25, 27] via regenerating the simulated maps with a further intermixing with the foreground components, reconstructing the signal, then correlating the reconstructed maps and constructing the correlation coefficients distribution. In this approach the distribution evaluation consisted of two steps only: the correlation map construction and the calculation of the pixel values distribution histogram.

A shift in the correlation coefficient distribution may be linked to an underestimation in the model used of the dust distribution in our Galaxy, where the excess in the negative coefficient values supports the hypothesis that in the corresponding pixels the correlated CMB and dust signals have an opposite sign. This fact can be used for the correction of dust component contribution. We are planning further studies of the detected bias.

4. ILC WMAP5 AND NVSS CORRELATION MAPS

Let us consider another correlation mapping application. Among the CMB map research works there are those dedicated to the dark matter studies using the Sachs-Wolfe integral effect [9], registered while correlating the CMB maps and the NVSS source distribution [28, 29].

The NVSS survey [5] is the most comprehensive Northern sky survey. It was conducted using the NRAO Very Large Array telescope (VLA) at a frequency of 1.4 GHz from 1993 to 1996, it has high sensitivity and covers the sky north of the declination $\delta = -40^\circ$ ($33884\square^\circ$ or 82% of the celestial sphere). This survey is actively used for various statistical studies in cosmology. The catalogue of this survey contains 1.8×10^6 sources and, according to it description, it is 99% complete up to the integrated flux densities over $S_{1.4\,\mathrm{GHz}} = 3.5$ mJy and 50% complete up to the flux densities of 2.5 mJy. The survey used the D–configuration of the VLA radiotelescope, and the size of the synthesized direction diagram in the half-power level, determining the resolution, constituted approximately $45''$. The survey data are available from the NRAO website[2], the virtual telescope SkyView[3] and from the CATS database[4] [30, 31].

Some non-Gaussian peculiarities were detected from the WMAP and NVSS data, poorly matching with the inflation ΛCDM model. Among them, for example, is the Cold Spot (CS), having the size of about 10° and the galactic coordinates of (l=209°, b=–57°). The CS, being statistically isolated in the CMB distribution, is one of the maps' particularities that contradict the hypothesis of homogeneous Gaussian background fluctuations. Originally, it was noted as a deviation from the Gaussian statistics while using the wavelet analysis [16, 18] for the first year data recorded by the WMAP mission. Subsequently, in the NVSS maps there was detected a significant dip of the radio source density of matter in the CS region [32], that allowed to hypothesize the existence of a Great Void 140 Mpc across, at redshift of $z < 1$, causing a gravitational anomaly leading to the integrated Sachs-Wolfe effect [9], and manifesting itself as a CS. At the same time there appeared some serious facts arguing that in this map at different angular scales there is some residual foreground components contribution, which produces the detected non-Gaussianity. This contribution may manifest itself in the earlier discovered link in the quadrupole between the cleaned CMB map and the galactic radiation components [26, 27] and, for another hand, determine the low multipole properties $\ell \leq 20$, resulting in their unstable reconstruction [25, 27]. Specifically, the CS particularities may be explained via the effects of these multipoles: the deviations of peak clusters statistics around the spot [33], namely, an increase in the the positive peaks number. An independent study of the properties of a spot, detected in the region with close coordinates on the maps and the radio source count in the NVSS survey [5], has demonstrated that the studied Cold Spot, with its gigantic size and its mere existence being difficult to explain in terms of the existing cosmological ΛCDM model, may as well be a simple statistical deviation, caused by the systematic effects [34].

Earlier we made a correlation analysis of the NVSS and WMAP5 surveys, preliminarily modifying the NVSS map making use of the method of one-dimensional sections for different angular scales

[2] http://www.cv.nrao.edu/nvss/

[3] http://skyview.gsfc.nasa.gov

[4] http://cats.sao.ru

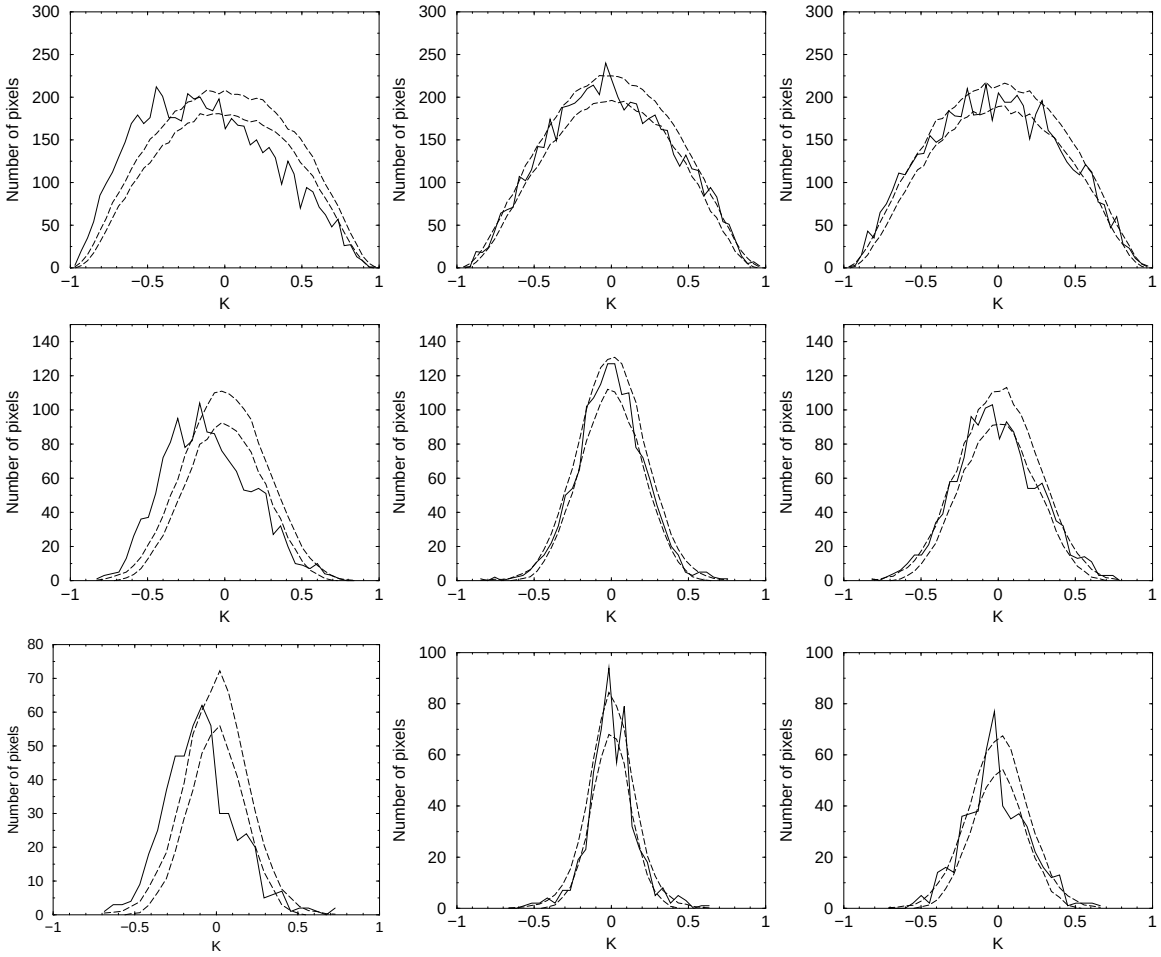

Figure 2: *Distribution of correlation index values in the pixels of the ILC and galactic foregrounds correlation maps: the dust radiation, the free-free and synchrotron emission (from left to right) for different correlation windows: 162′ , 324′ and 540′ (from top to bottom). The admissible limits of correlation level, constructed on the modelling data, are shown with dashed lines.*

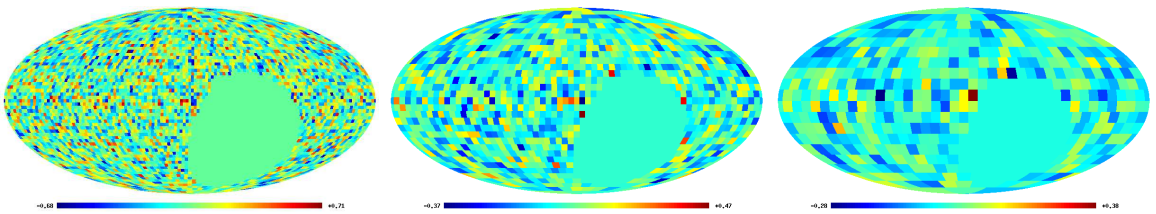

Figure 3: *ILC and NVSS correlation maps for different correlation windows: 162′ , 324′ and 540′ (from right to left). In the right bottom part of each figure there is an screened area, which was not considered in our analysis due to the lack of NVSS observations in the $\delta < -40^\circ$ range.*

[22]. To construct the modified NVSS map, we used a characteristic, represented by a mean square of the source flux density in an area of given dimensions with the center at the pixel, determined by the selected area. As a result we discovered that the correlation statistics in the studied scales (0.75°, 3°, 4.5°, and 6.75°) does not vary from the expected random maps. Therefore, we may conclude that the found correlations may be caused by a statistical coincidence.

In the present work we carried out the mapping of the correlation properties on the sphere using the same data from WMAP5 and NVSS. The re-

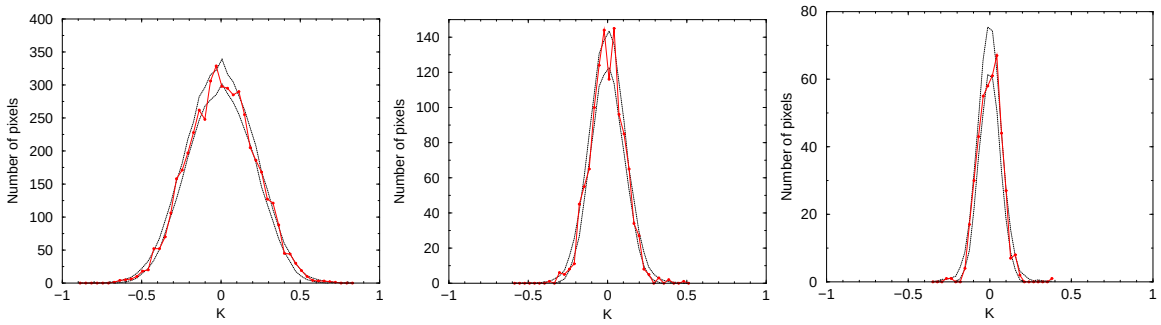

Figure 4: *Distribution of correlation index values in the pixels of the ILC and NVSS correlation maps for different correlation windows: 162′ , 324′ , and 540′ (from right to left). The admissible limits of the correlation level, constructed using the modelling data, are shown by the dashed lines.*

sults are shown on Fig. 3 and 4. While analyzing the map statistics (Fig. 4) we were taking into account the absence of NVSS data in the declination area of $\delta < -40°$. The NVSS map was constructed using two methods: (1) via computing the number of sources in every pixel and (2) via summing up the flux densities of the radio sources, contained in the pixel area. As the correlation properties are practically undistinguishable (the difference of less than 1%), we shall demonstrate the whole analysis for the first case.

As we can see from Fig. 4, the statistics of the correlated pixel values lies within the admissible random deviations, what confirms the earlier estimations [22]. This implies that in the correlation coefficient distribution no signal is found with a level higher than 1σ on the given scales, caused by, for example, an interaction with the large-scale structure and dark energy, manifesting themselves through the Sachs-Wolfe effect. On the other hand, as the coefficient distribution corresponds to the expected random deviations for the Gaussian disturbances in the ΛCDM model, we may arrive at a conclusion that there exists an infinitesimal number of separated non-Gaussian spots, if any at all. And allowing for the fact that the Cold Spot itself might be the result of a local modulation of spherical harmonics, that appeared as a consequence of the component separation [33], we may construe that this phenomenon, observed simultaneously in CMB and NVSS, is most likely not an anomaly but may be a systematism (foreground overestimation) while analysing the WMAP data and a random coincidence with a statistically insignificant peculiarity of the NVSS distribution.

5. CONCLUSION

We have presented here a method of correlation mapping on the sphere for a given angular scale. This method is software-implemented within the framework of the GLESP package. The proposed method allows analyzing on the sphere the properties of a random CMB signal having a single realisation based on its statistical characteristics only, namely, on its ergodicity, when taking a multitude of CMB realisations in different regions of the sphere, we can make a conclusion about its realisation in a multitude of similar Universes, and, in so doing, evaluate its probable values. We have demonstrated the capabilities of our method for the WMAP5 data (the maps of ILC and foreground radiations: synchrotron, free-free and dust). For the correlation maps constructed, we discovered a shift in the pixel value distribution in favour of anti-correlations for dust and synchrotron radiation on the scales of 162′, 324′, and 540′. This calls for a possible overestimation of the contribution of these foregrounds in the method of ILC components separation. An excess in the negative coefficient values indicates that in the corresponding pixels, the correlated signals of CMB and dust have an opposite sign. This fact may be used while correcting the contribution of the dust component. We are planning further studies of this issue.

The described approach was as well used for a study of correlation properties of the CMB and NVSS maps. In the correlation coefficient distribution there was found no additional signal a level higher than 1σ over the one expected in the event of a random agreement of Gaussian disturbances in the ΛCDM cosmological model. Such a distribution of correlations argues for the fact that the Cold Spot, observed both in the CMB and NVSS, may be in fact the result of a random coincidence, and there is no need invoking new physics to explain it.

Acknowledgments. We would like to thank NASA for the chance to use its Legacy Archive for Microwave Background Data Analysis from which we retrieved the WMAP data. We are as well grateful to the authors of the

HEALPix[5] [35] package using which we converted the WMAP maps into the $a_{\ell m}$ coefficients. In our work we used the GLESP[6] [23, 24] package for the further analysis of the CMB data on the sphere and the FADPS[7] [36, 37] one-dimensional data processing system. The present work was supported by the Leading Scientific Schools of Russia grant and the Russian Foundation for Basic Research (project Nos. 09-02-00298 and 09-02-92659-IND). O.V.V. as well acknowledges the partial support of the RFBR (project No. 08-02-00159).

References

[1] C. L. Bennett, M. Halpern, G. Hinshaw, et al., Astrophys. J. Supp. **148**, 1 (2003); astro-ph/0302207.
[2] G. Hinshaw, J. L. Weiland, R. S. Hill, et al., Astrophys. J. Supp., submitted, (2008); arXiv:0803.0732.
[3] E. Komatsu, J. Dunkley, M. R. Nolta, et al., Astrophys. J. Supp., submitted, (2008); arXiv:0803.0547.
[4] M. F. Skrutskie, S. E. Schneider, R. Stiening, et al., in *The Impact of Large Scale Near-IR Sky Surveys*, Ed. by F. Garzon et al. (Kluwer Acad. Publ. Comp., Dordrecht 1997) p.25.
[5] J. J. Condon, W. D. Cotton, E. W. Greisen, et al., AJ **115**, 1693 (1998).
[6] D. P. Schneider, P. B. Hall, G. T. Richards, et al., AJ **134**, 102 (2007).
[7] K. M. Huffenberger , H. K. Eriksen, and F. K. Hansen, Astrophys. J **651L**, 81 (2006); astro-ph/0606538.
[8] O. V. Verkhodanov and Yu. N. Parijskij, *Radio galaxies and Cosmology*, (Fiz.Mat.Lit., Moscow 2009) [in Russian] (in press).
[9] R. K. Sachs and A. M. Wolfe, Astrophys. J **147**, 73 (1967).
[10] R. A. Sunyaev and Ya. B. Zeldovich, Astrophys. Sp. Sci. **7**, 3 (1970).
[11] P. D. Naselsky, A. G. Doroshkevich, and O. V. Verkhodanov, Astrophys. J **599**, L53 (2003); astro-ph/0310542.
[12] P. D. Naselsky, A. G. Doroshkevich, and O. V. Verkhodanov, MNRAS **349**, 695 (2004); astro-ph/0310601.
[13] L.-Y. Chiang, P. D. Naselsky, O. V. Verkhodanov, and M. J. Way, Astrophys. J **590**, L65 (2003); astro-ph/0303643.
[14] P. Coles, P. Dineen, J. Earl, and D. Wright, MNRAS **350**, 989 (2004); astro-ph/0310252.
[15] C. J. Copi, D. Huterer, and G. D. Starkman, Phys. Rev. D **70**, 043515 (2004); astro-ph/0310511.
[16] P. Vielva, E. Martinez-Gonzalez, R. B. Barreiro, et al., Astrophys. J **609**, 22 (2004), astro-ph/0310273.
[17] P. Mukherjee and Y. Wang, Astrophys. J **613**, 51 (2004).
[18] M. Cruz, E. Martinez-Gonzalez, P. Vielva, and L. Cayon, MNRAS **356**, 29 (2005).
[19] H. K. Eriksen, D. I. Novikov, P. B. Lilje, et al., Astrophys. J **612**, 64 (2004).
[20] C.-G. Park, C. Park, and J. R. Gott III, Astrophys. J **660**, 959 (2006); astro-ph/0608129.
[21] M. L. Khabibullina, O. V. Verkhodanov, and Yu. N. Parijskij, Astrophys. Bull. **63**, 101 (2008).
[22] O. V. Verkhodanov, M. L. Khabibullina, E. K. Majorova, and Yu. N. Parijskij, Astrophys. Bull. **63**, 366 (2008).
[23] A. G. Doroshkevich, P. D. Naselsky, O. V. Verkhodanov, et al., Int. J. Mod. Phys. D **14**, 275 (2003); astro-ph/0305537.
[24] O. V. Verkhodanov, A. G. Doroshkevich, P. D. Naselsky, et al., Bull. Spec. Astrophys. Obs. **58**, 40 (2005).
[25] P. D. Naselsky, O. V. Verkhodanov, and M. T. B. Nielsen, Astrophys. Bull. **63**, 216 (2008); arXiv:0707.1484.
[26] P. D. Naselsky and O. V. Verkhodanov, Int. J. Mod. Phys. D **17**, 179 (2008); astro-ph/0609409.
[27] P. D. Naselsky and O. V. Verkhodanov, Astrophys. Bull. **62**, 218 (2007).
[28] M. R. Nolta, E. L. Wright, L. Page, et al., Astrophys. J **608**, 10 (2004); astro-ph/0305097.
[29] J. D. McEwen, P. Vielva, M. P. Hobson, et al., MNRAS **376**, 1211 (2007); astro-ph/0602398.
[30] O. V. Verkhodanov, S. A. Trushkin, H. Andernach, and V. N. Chernenkov, in *Astronomical Data Analysis Software and Systems VI*, Ed. by G. Hunt and H. E. Payne, ASP Conf. Ser. **322**, 46 (1997).
[31] O. V. Verkhodanov, S. A. Trushkin, H. Andernach, and V. N. Chernenkov, Bull. Spec. Astrophys. Obs. **58**, 118 (2005); arXiv:0705.2959.
[32] L. Rudnick, S. Brown, and L. R. Williams, Astrophys. J **671**, 40 (2007); arXiv:0704.0908.
[33] P. D. Naselsky, P. R. Christensen, P. Coles, et al., (2007); arXiv:0712.1118.
[34] K. M. Smith and D. Huterer, arXiv:0805.2751
[35] K. Górski, E. Hivon, A. J. Banday, B. D. Wandelt, et al., Astrophys. J **622**, 759 (2005).
[36] O. V. Verkhodanov, in *Astronomical Data Analysis Software and Systems VI*, Ed. by G. Hunt and H. E. Payne, ASP Conf. Ser., **125**, 46 (1997).
[37] O. V. Verkhodanov, B. L. Erukhimov, M. L. Monosov, et al., Bull. Spec. Astrophys. Obs. **36**, 132 (1993).

[5] http://www.eso.org/science/healpix/
[6] http://www.glesp.nbi.dk
[7] http://sed.sao.ru/∼vo/fadps_e.html

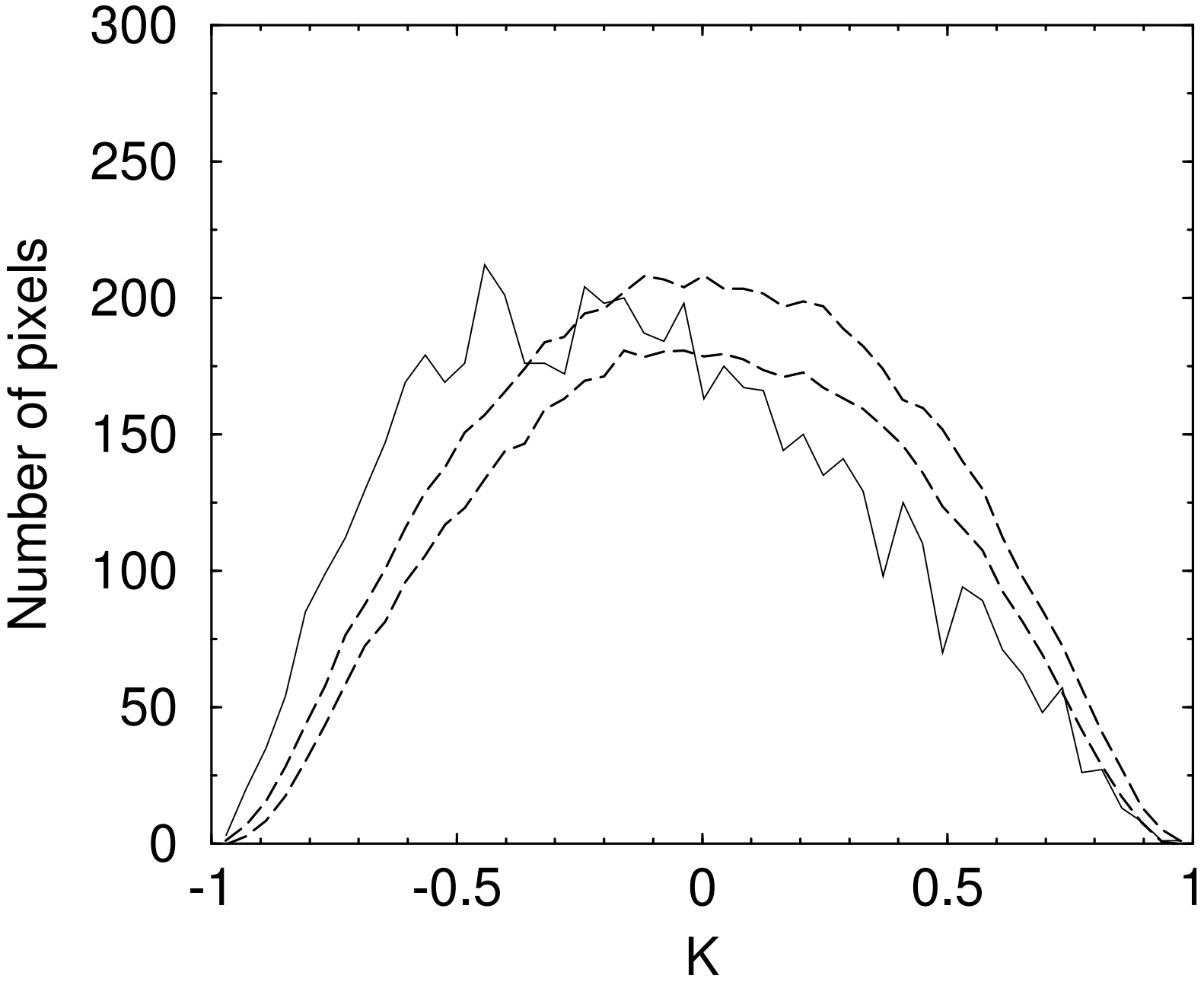
300
250
200
150
100
50
0
Number of pixels
-1
-0.5
0
0.5
1
K

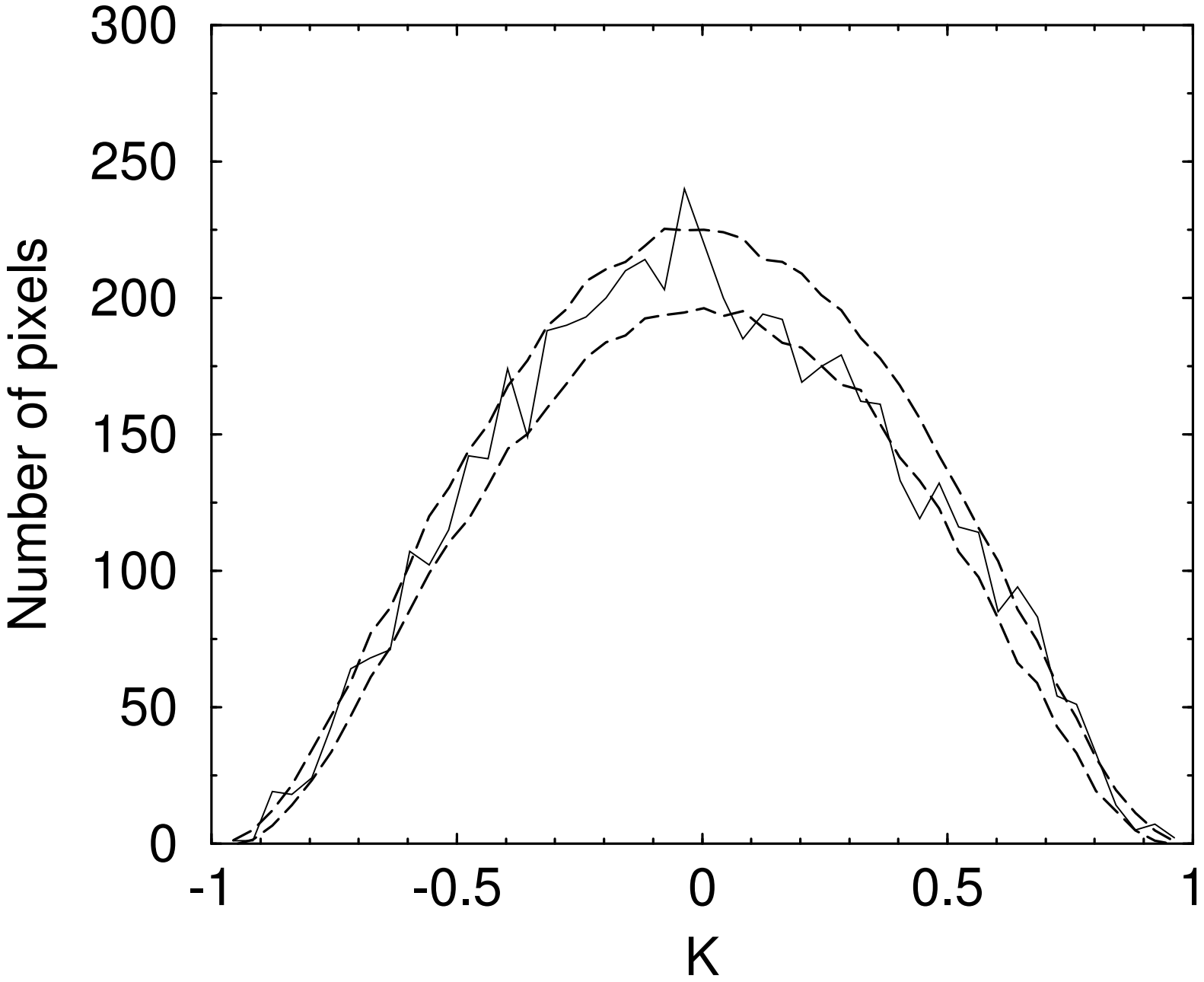
300
250
200
150
100
50
0
Number of pixels
-1
-0.5
0
0.5
1
K

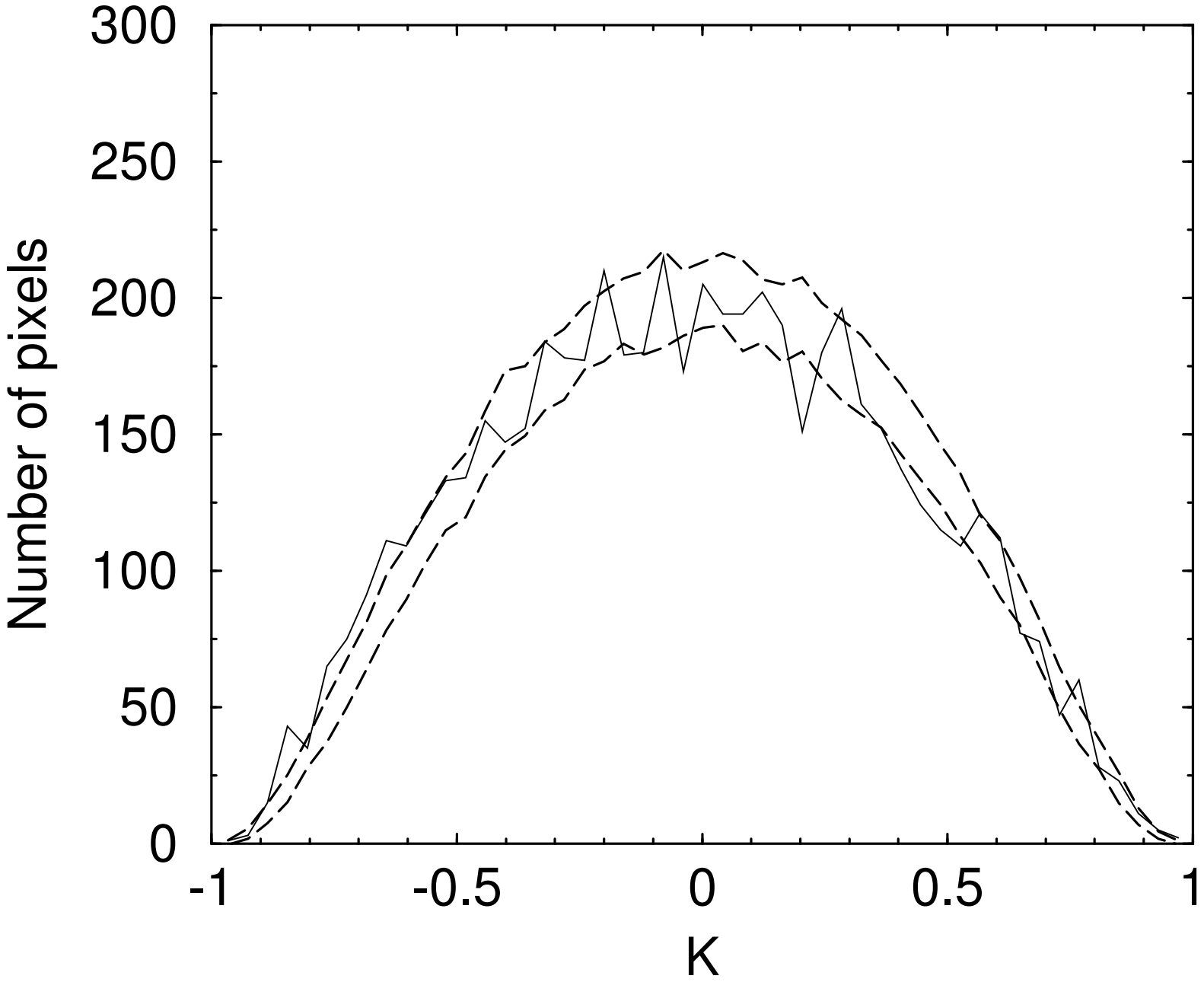
300
250
200
150
100
50
0
Number of pixels
-1
-0.5
0
0.5
1
K

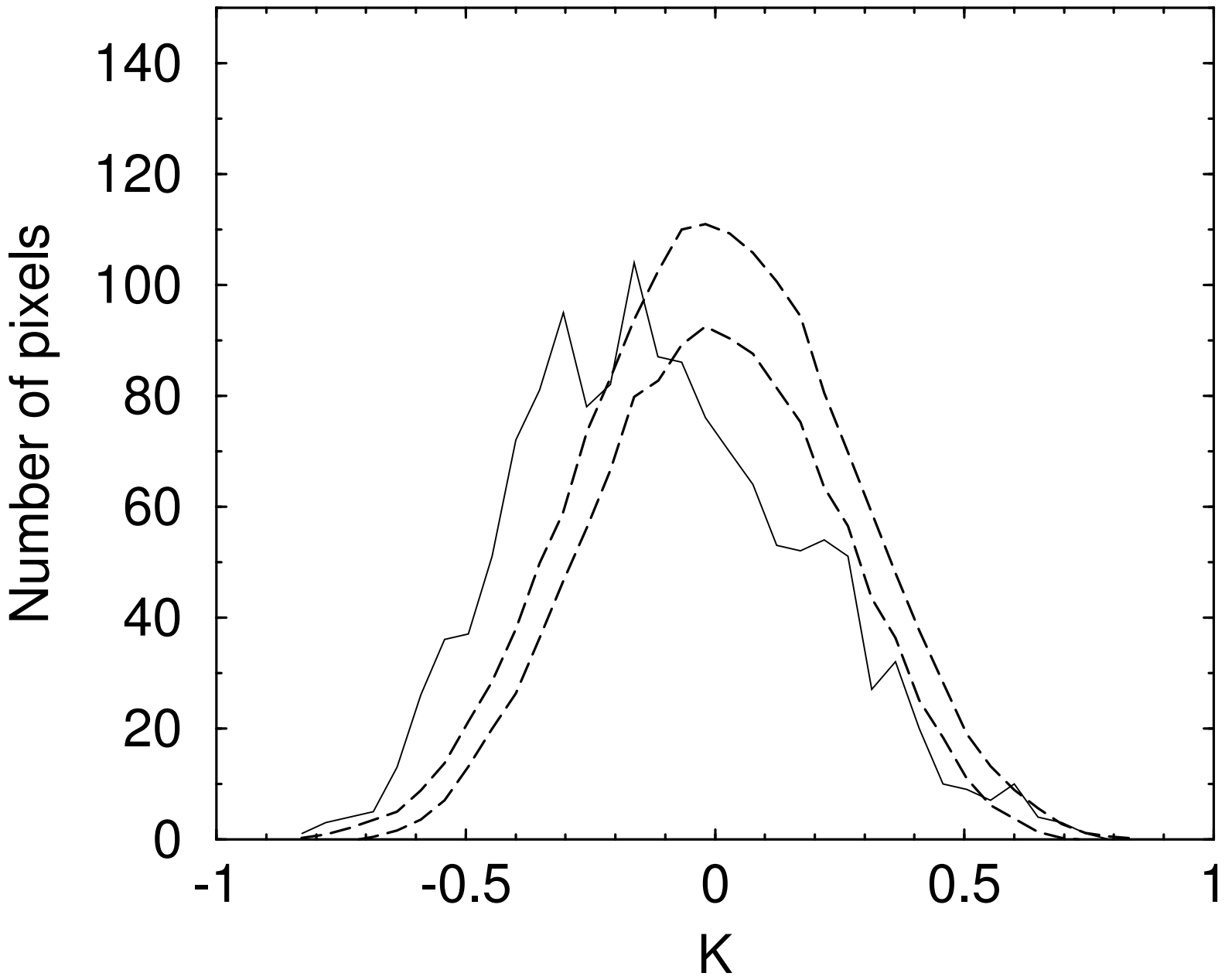
Number of pixels
140
120
100
80
60
40
20
0
-1
-0.5
0
0.5
1
K

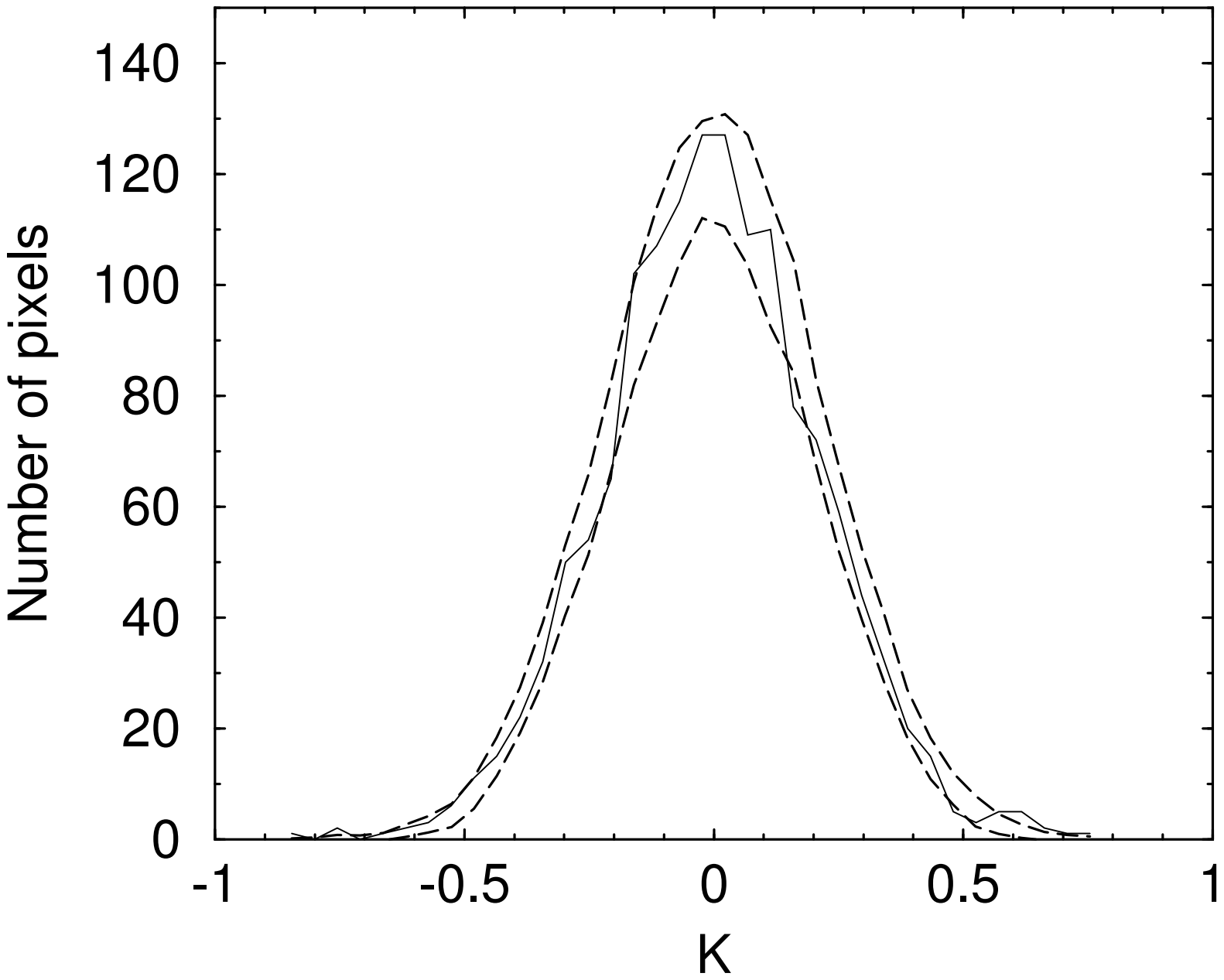
Number of pixels
140
120
100
80
60
40
20
0
-1
-0.5
0
0.5
1
K

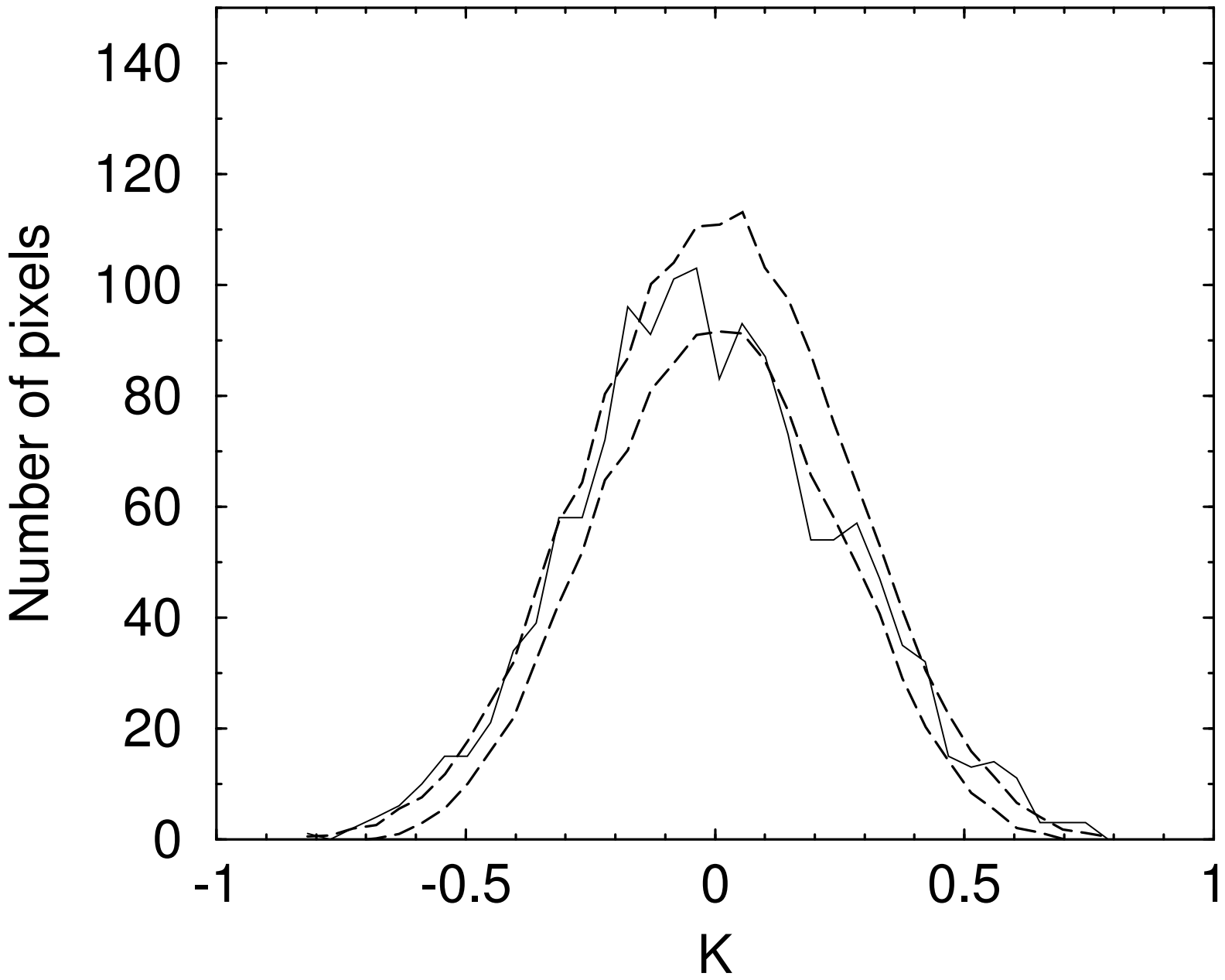
Number of pixels
140
120
100
80
60
40
20
0
-1
-0.5
0
0.5
1
K

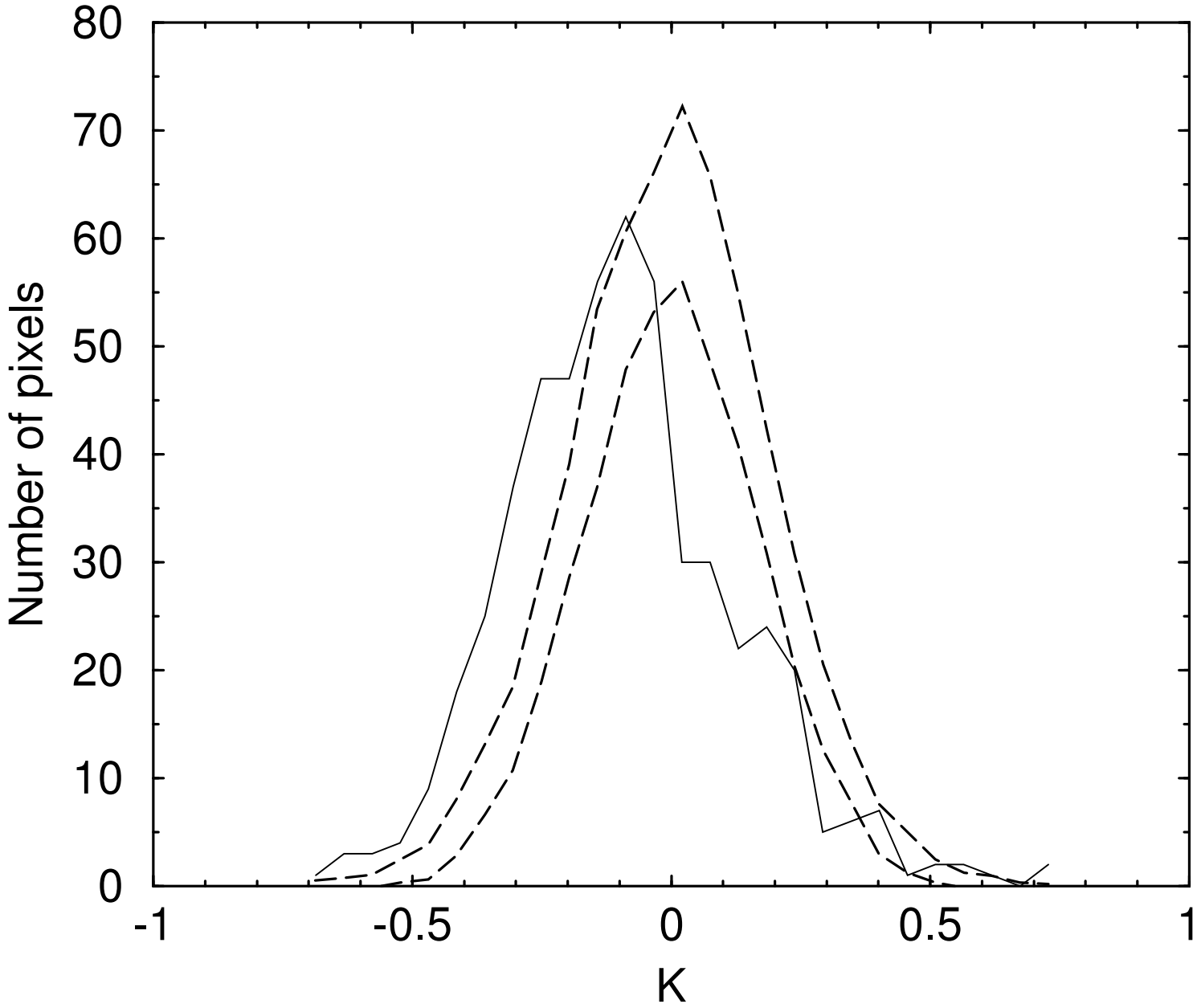
80
70
60
50
40
30
20
10
0
Number of pixels
-1
-0.5
0
0.5
1
K

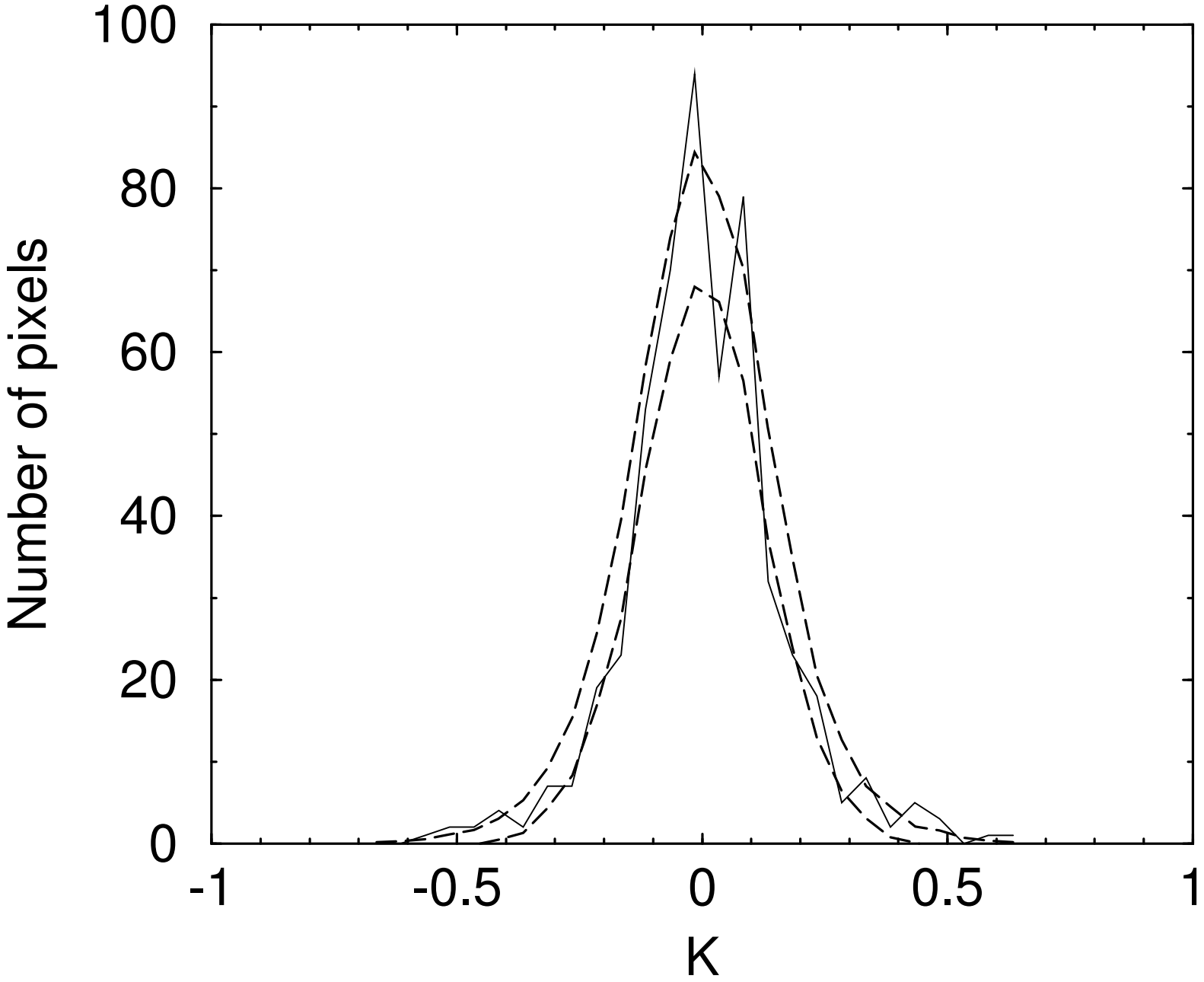
100
80
60
40
20
0
Number of pixels
-1
-0.5
0
0.5
1
K

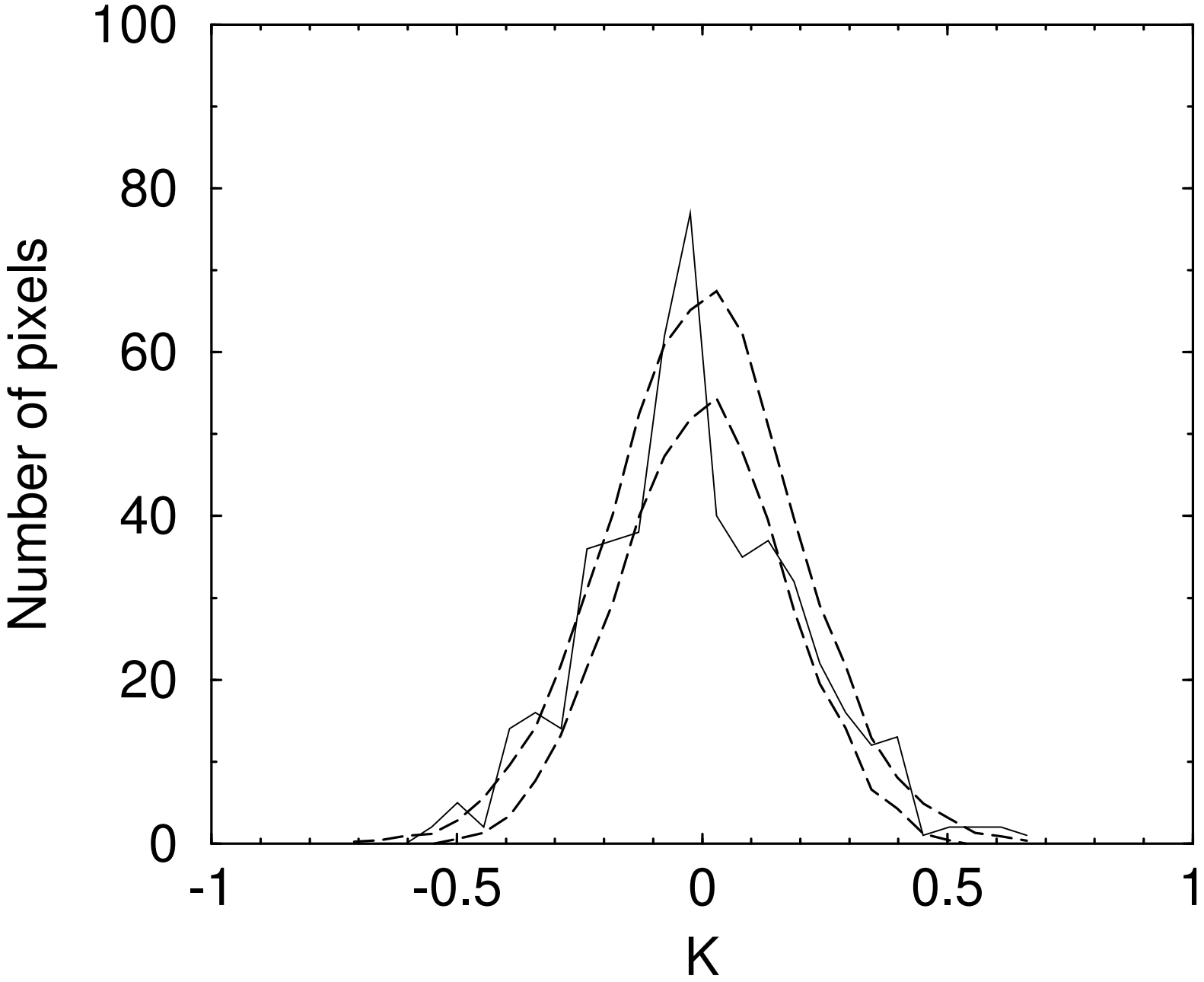
100
80
60
40
20
0
Number of pixels
-1
-0.5
0
0.5
1
K